Journal of the Korean Physical Society, Vol. 77, No. 5, September 2020, pp. 429∼437

FEL Simulation of New Hard X-ray Undulator Line at PAL-XFEL

Chi Hyun Shim* and Heung-Sik Kang
Pohang Accelerator Laboratory, Pohang University of Science and Technology, Pohang 37673, Korea

(Received 7 January 2020; revised 5 April 2020; accepted 6 April 2020)

The Pohang Accelerator Laboratory X-ray Free Electron Laser (PAL-XFEL) has been successfully operating as a remarkably-stable XFEL facility in the world. The hard X-ray beamline, however, has only one undulator line (HX1) with a 26-mm undulator period for which the maximum undulator parameter K is 1.87. The lowest photon energy that can be generated from the HX1 with a maximum electron beam energy at PAL-XFEL (10.5 GeV) is about 14.65 keV. When a lower photon energy than that is required by the beamline users, the electron beam energy has to be decreased, which results in a decreased accessible FEL pulse energy. Therefore, a new hard X-ray undulator line (HX2) with a higher undulator parameter K is needed to make full use of the PAL-XFEL performance in the lower photon energies by increasing the resonant electron beam energy. The undulator period of the HX2 is decided as 35 mm by using Ming Xie's fitting formula to estimate the performance of the HX2. FEL simulations with the GENESIS code are carried out to evaluate the performance of the HX2, including the effect of the post-saturation region. The undulator tapering configuration is optimized by maximizing the FEL intensity for each case. We show that the radiation power at the end of the HX2 can be increased up to 2.5 times higher than that of the HX1 over the entire target photon-energy range of the HX2 ($2 \sim 10$ keV) by utilizing an undulator with a longer period and a higher undulator parameter K.

Keywords: PAL-XFEL, Free-electron laser, Self-amplified spontaneous emission, Hard X-ray
DOI: 10.3938/jkps.77.429

I. INTRODUCTION

The X-ray Free Electron Laser (XFEL) is a novel and unique tool which can open new frontiers in X-ray science; only five hard X-ray FEL facilities exist in the world [1–5]. The Pohang Accelerator Laboratory X-ray Free Electron Laser (PAL-XFEL), which is one of those facilities, has been successfully operating and is a remarkably-stable XFEL facility [3,6,7]. A large number of scientists investigate the unrevealed phenomena by using the PAL-XFEL and they are starting to obtain significant results [8–11].

For the hard X-ray beamline, however, one undulator line with a 26-mm undulator period for which the maximum undulator parameter K is 1.87 is available [6]. The lowest photon energy that can be generated from the HX1 with a maximum electron beam energy at the PAL-XFEL (10.5 GeV) is about 14.65 keV. For a self-amplified spontaneous emission (SASE) FEL, the FEL parameter ρ is the extraction efficiency of the FEL, and the saturation power is about ρ times the electron beam power [12]. Note that the electron beam power is the product of the electron beam energy and the current of the electron beam. When a photon energy lower than 14.65 keV is required by the beamline users, the electron beam energy has to be decreased from 10.5 GeV, which results in decreased accessible FEL pulse energy. Therefore, a new hard X-ray undulator line (HX2) with a higher undulator parameter K is needed to make full use of the PAL-XFEL performance at lower photon energies by increasing the resonant electron beam energy. The HX2 can be installed in the vacant space beside the existing undulator line as shown in Fig. 1.

In this paper, the undulator period of the HX2 is decided by using Ming Xie's fitting formula to estimate the performance of the HX2 [13,14]. FEL simulations with the GENESIS code [15] are carried out to evaluate the performance of the HX2, including the effect of the post-saturation region. The undulator tapering configuration is optimized by maximizing the FEL intensity for each case [16–18].

II. UNDULATOR PERIOD FOR THE HX2

According to the resonance condition of undulator which is described as follows [12], the undulator period or the undulator parameter has to be increased to maintain the resonant photon energy when the electron beam energy is also increased:

$$\lambda_{\mathrm{r}} = \frac{\lambda_{\mathrm{u}}}{2\gamma^2}\left(1 + \frac{K^2}{2}\right) , \qquad (1)$$

*E-mail: sch0914@postech.ac.kr

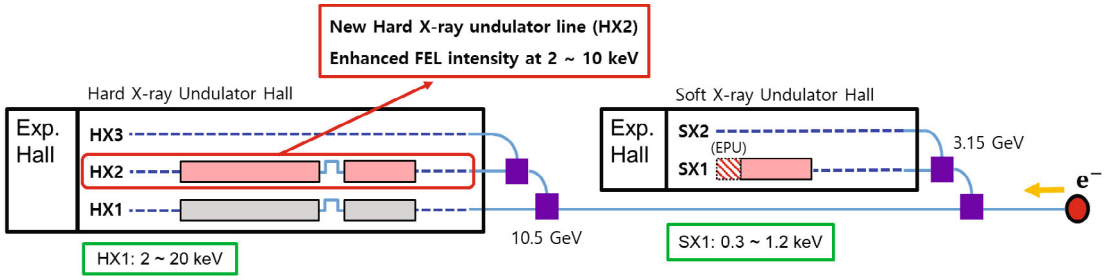

Fig. 1. Layout of the PAL-XFEL undulator lines. Two undulator lines (HX1 for hard X-rays and SX1 for soft X-rays) are in operation, and three undulator lines (HX2, HX3, SX2) will be available in the future. A new undulator line for hard X-rays is proposed for the HX2, which is indicated by the red box.

λ_r is the resonant wavelength, γ is the Lorentz factor, which is obtained by dividing the electron beam energy by the electron's rest mass energy, and K is the undulator parameter. Note that the photon energy of radiation (E_{ph}) can be obtained by using the simple relation E_{ph} [keV] $= 1.24/\lambda_r$ [nm]. In the case of an undulator which uses a permanent magnet, the undulator parameter K is related to the undulator period and the undulator gap and is calculated by using Halbach's formula [13], which is

$$K = 320 \cdot \lambda_u \cdot \exp\left(-5.08\frac{g}{\lambda_u} + 1.54\left(\frac{g}{\lambda_u}\right)^2\right) \quad . \quad (2)$$

At the PAL-XFEL, the electron beam energy can be increased to 11 GeV, which was demonstrated and approved by Korea Institute of Nuclear Safety (KINS). However, this is too close to the boundary condition of the PAL-XFEL; therefore, 10.5 GeV is considered as the stable maximum electron beam energy for the FEL lasing condition. The maximum undulator parameter K for λ_u = 26 mm, which is used for the HX1 at the PAL-XFEL, is 1.87 and the corresponding undulator gap from Eq. (2) is 8.478 mm. A sufficient undulator gap for an out-vacuum undulator is necessary to reserve sufficient space for the vacuum pipe; therefore, the maximum undulator parameter K for other undulator periods is determined by the minimum undulator gap of the undulator for λ_u = 26 mm.

When the maximum electron beam energy and the minimum undulator gap are limited, the electron beam energy and the undulator parameter K for a certain undulator period can be decided by using Eq. (1) and (2) to generate the specific photon energy, as shown in Fig. 2. In the figure, a kinked point appears where both the maximum electron beam energy and the maximum undulator parameter K are needed for a certain resonant photon energy. The electron beam energy has to be decreased while the undulator parameter K is maintained at its maximum value to satisfy the resonance condition at photon energies lower than the energy associated with the kinked point. In contrast, the undulator parameter K has to be decreased by opening the undulator gap while the electron beam energy is maintained at its maximum value to satisfy the resonance condition at photon energies higher than the energy associated with the kinked point.

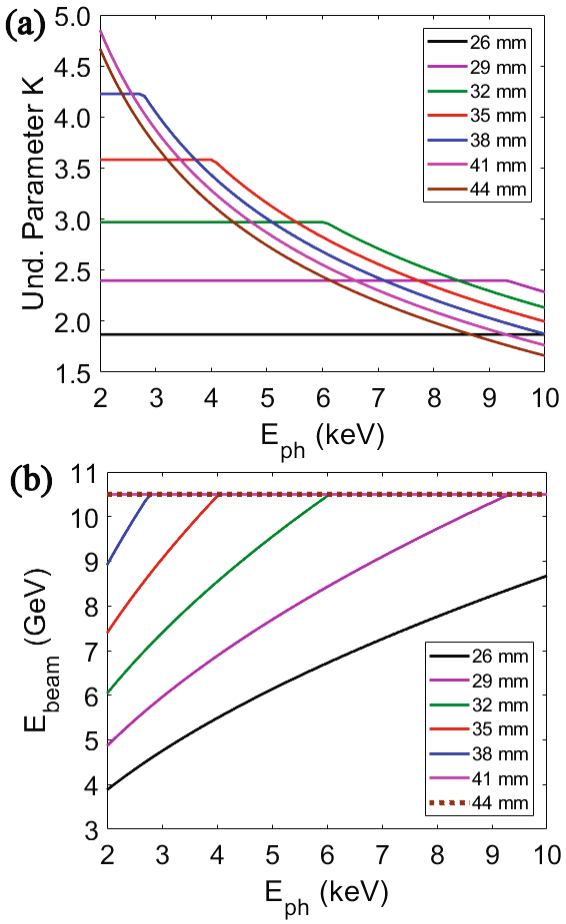

Fig. 2. (a) Undulator parameter K and (b) energy of the electron beam vs. the resonant photon energy for various undulator periods. The individual value of the undulator periods are indicated by the legend in the figure. The maximum energy of the electron beam and the minimum gap of the undulator are limited to 10.5 GeV and 8.478 mm, respectively.

When the undulator period is increased, the maximum

Table 1. Main parameters for PAL-XFEL.

Parameter	Value	Unit
Max. electron beam energy	10.5	GeV
Normalized slice emittance	0.4	mm-mrad
Peak current	3	kA
Slice energy spread	1.5	MeV
Length of half FODO cell (from quadrupole to next quadrupole)	~ 6	m
Quadrupole B field	3.12	T
Length of undulator	~ 5	m
Number of undulators	20	
Max. K for $\lambda_u = 26$ mm (HX1)	1.87	
Max. K for $\lambda_u = 35$ mm (HX2)	3.4	

undulator parameter K is also increased, as shown in Fig. 2(a). When a longer undulator period is used, a higher electron beam energy can be used to generate the same photon energy of radiation, as shown in Fig. 2(b). Note that a 10.5-GeV electron beam energy is used over the entire range of photon energies for undulator periods $\geq$ 41 mm.

If the undulator period for the HX2 is to be determined, performance of the undulator line, such as the saturation power and the saturation length, has to be estimated for various undulator periods. When Ming Xie's fitting formula [13,14] is used with the parameters indicated in Fig. 2 and listed in Table 1, the saturation power and the saturation length can be calculated. Because the main objective of the HX2 is FEL intensity enhancement at photon energies $\leq$ 10 keV in comparison with the HX1, the ratios of the saturation power and the saturation length to the case for which the undulator period is 26 mm (HX1) are shown in Fig. 3.

As shown in Fig. 3(a), the lower the generated photon energy of radiation is, the more the ratio of the saturation power is increased. However, the ratio of the saturation power for photon energies lower than the energy of the kinked point stays at a certain value. When the undulator period is increased, the photon energy of the kinked point moves toward lower photon energy, and the certain value is also increased. A long undulator period seems to be more preferable for enhancing the radiation power. Note that the kinked point does not appear in the cases with undulator periods $\geq$ 41 mm because the maximum electron beam energy is used over the entire target photon-energy range of the HX2 ($2 \sim 10$ keV), as shown in Fig. 2(b).

However, the longer the undulator period is, the longer the saturation length that is required over the entire range of photon energies is, as shown in Fig. 3(b). Even though a similar saturation power at a photon energy higher than that of the kinked point can be obtained with different undulator periods, the saturation length

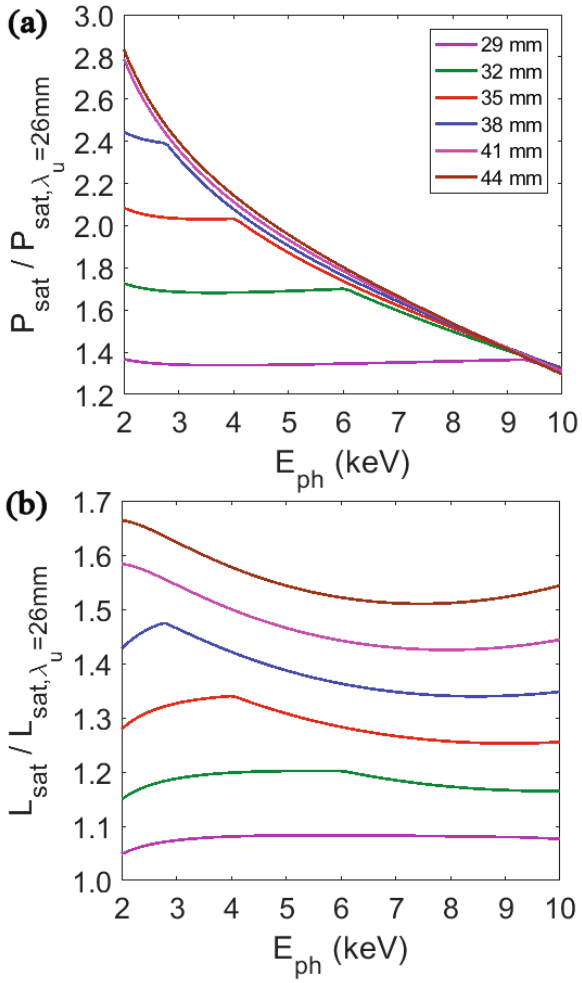

Fig. 3. Ratios of (a) the saturation power and (b) the saturation length to the case in which the undulator period is 26 mm (HX1) vs. the resonant photon energy for various undulator periods. Individual values of the undulator periods are indicated by the legend in the figure. The saturation power and the saturation length are estimated by using Ming Xie's fitting formula. The parameters indicated in Fig. 2 and listed in Table 1 are used to estimate the values.

is still increased when the undulator period is increased. Such a delayed saturation reduces the possibility of a radiation power enhancement in the post-saturation region by undulator tapering. Therefore, the undulator period is moderately increased to obtain sufficient radiation power enhancement with an acceptable saturation length.

At the PAL-XFEL, two types of undulators, one with a 26-mm undulator period and the other with a 35-mm undulator period were developed and have been used for the HX1 and the SX1, as shown in Fig. 1 [19]. Plots of the measured undulator parameter K vs. undulator gap for the two undulators are shown in Fig. 4. When the undulator with a 35-mm undulator period is used for the HX2, we estimate that the saturation power can be

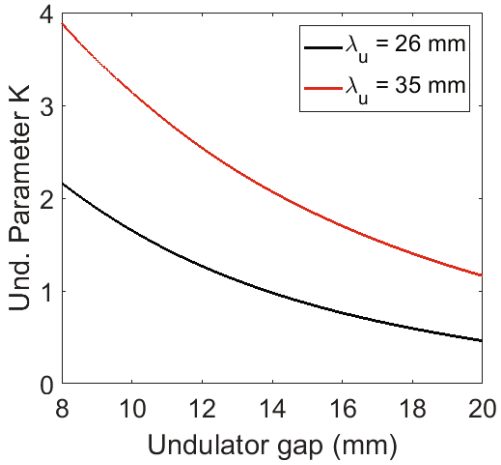

Fig. 4. Measured undulator parameter K vs. undulator gap for the two types of undulators developed at the PAL-XFEL. The undulator with a 26-mm undulator period (λ_u) is used for the HX1 (black line), and the undulator with a 35-mm λ_u is used for the SX1 (red line).

increased up to twice that from the HX1 over the entire target photon-energy range of the HX2 (2 $\sim$ 10 keV), as shown by the red line in Fig. 3(a). The saturation length is also increased to about 30% longer than that of the HX1, as shown by red line in Fig. 3(b), which is sufficiently acceptable for the PAL-XFEL. Moreover, no additional R&D is required for the undulator, so considerable time and money can be saved. Therefore, the undulator with a 35-mm undulator period is suitable for the HX2.

III. PERFORMANCE ESTIMATE FOR THE HX2

Because the HX1 and the HX2 are located in the same area, as shown in Fig. 1, the same properties of the electron beam are shared when the two undulator lines are operated simultaneously. In that case, the electron beam energy is determined by the resonant photon energy at the HX1. A sufficiently high electron beam energy may be accessible at the HX2 when a high photon energy is used at the HX1; however, a quite low electron beam energy should be used at the HX2 when the photon energies at the two undulator lines are similar.

Therefore, two conditions at the HX2 have to be considered to identify fully the performance of the HX2: One condition is that the electron beam energy be increased as high as possible for the HX2 as shown in Fig. 2. The other condition is that the resonant photon energies at the HX1 and the HX2 be the same. In this case, the electron beam energy is decreased to satisfy the resonance condition at the HX1, so the undulator parameter K of the HX2 has to be decreased to satisfy the resonance condition with low electron beam energy. These

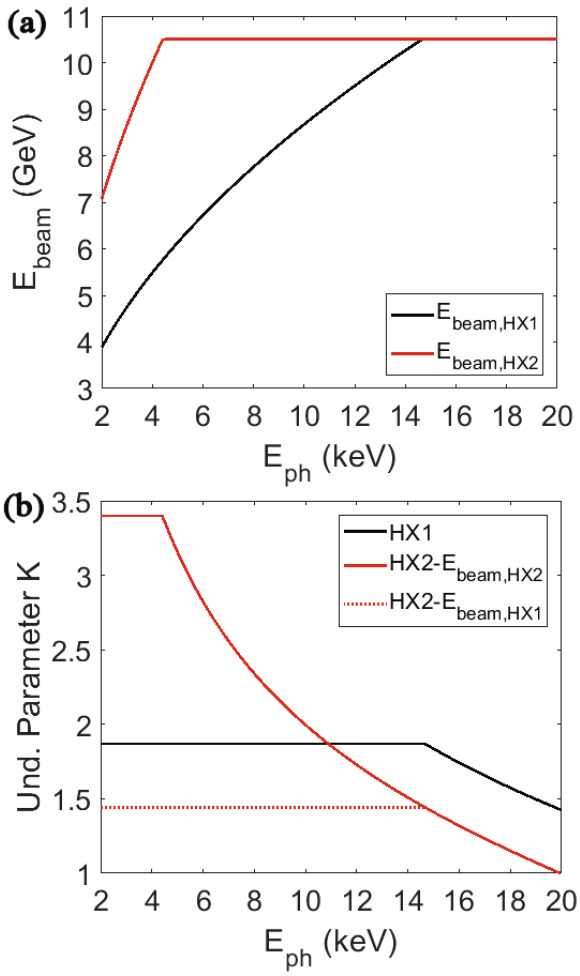

Fig. 5. (a) Energy of the electron beam and (b) undulator parameter K vs. the resonant photon energy for the HX1 (λ_u = 26 mm, black solid line) and for the HX2 (λ_u = 35 mm, red solid line). The red-dotted line indicates the HX2 with an electron beam energy for the same photon energy at the HX1. The maximum values of the undulator parameter K for the HX1 and the HX2 are limited to 1.87 and 3.4, respectively.

two conditions represent the boundaries of the highest and the lowest performances at the HX2.

The electron beam energy and the undulator parameter K vs. the resonant photon energy for these conditions are shown in Fig. 5. The maximum values for the undulator parameter K of the HX1 (λ_u = 26 mm) and the HX2 (λ_u = 35 mm) are limited to 1.87 and 3.4, respectively, for stable operation. From Fig. 4, the values of the undulator gap corresponding to that undulator parameter K are 9.0768 mm and 9.2426 mm, which are sufficiently wide for the vacuum pipe.

In the case of the HX1, the maximum electron beam energy (10.5 GeV) is used at photon energies higher than 14.7 keV, as shown by the black solid line in Fig. 5(a). Until that photon energy, the electron beam energy is increasing while the undulator parameter K of HX1 is staying at 1.87, as shown by the black solid line in Fig. 5(b).

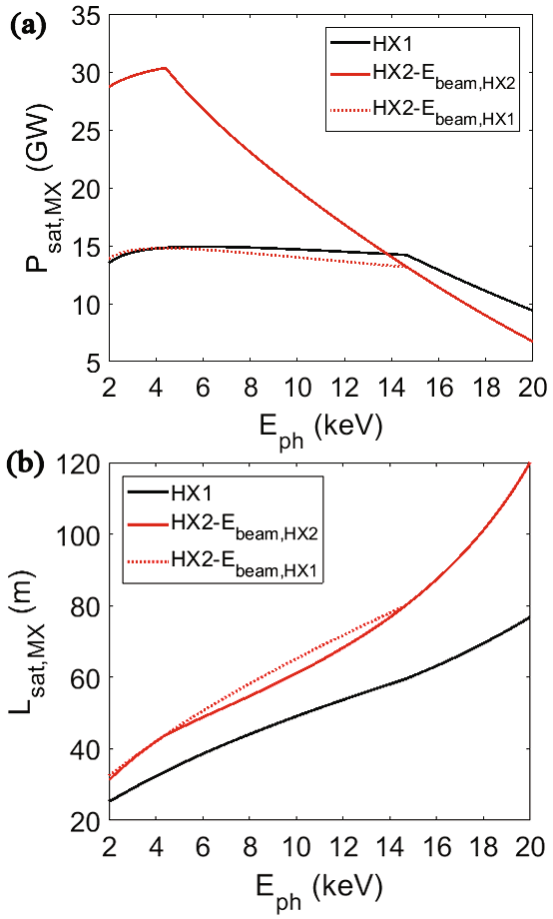

Fig. 6. (a) Saturation power and (b) saturation length vs. the resonant photon energy for the HX1 (λ_u = 26 mm, black solid line) and for the HX2 (λ_u = 35 mm, red solid line). The red-dotted line indicates the HX2 with an electron beam energy for the same photon energy at the HX1. The saturation power and the saturation length are estimated by using Ming Xie's fitting formula. The parameters indicated in Fig. 5 and listed in Table 1 are used to estimate the values.

After that photon energy, the undulator parameter K is decreasing as the undulator gap is opening.

In the case of the HX2, the maximum electron beam energy is used at photon energies higher than 4.5 keV, as shown by the red solid line in Fig. 5(a). Until that photon energy, the electron beam energy is increasing while the undulator parameter K of HX2 is staying at 3.4, as shown by the red solid line in Fig. 5(b). After that photon energy, the undulator parameter K is decreasing to satisfy the resonance condition. When the same photon energies are used in both undulator lines, however, the electron beam energy used at the HX2 is the same at that used at the HX1, as shown by the black solid line in Fig. 5(a). The undulator parameter K of the HX2 is also adjusted to satisfy the resonance condition, as shown by the red dotted line in Fig. 5(b). In this case, the undulator parameter K of the HX2 stays at 1.4434 until the photon energy reaches 14.7 keV.

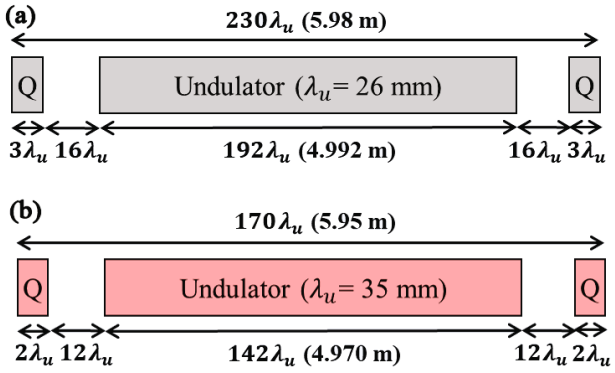

Fig. 7. Undulator lattice units for (a) the HX1 and (b) the HX2. Q means half of a quadrupole magnet. The drift spaces at both ends of the undulator are necessary for installing the devices to diagnose the status, focus the transverse beam size, and adjust the phase of the electron beam.

To estimate the performance of the HX2 for the two conditions, we use Ming Xie's fitting formula [13,14] with parameters presented in Fig. 5 and listed in Table 1 to calculate the saturation power and the saturation length, and we show the results in Fig. 6. By virtue of the high electron beam energy, the saturation power of the HX2, which is indicated by the red solid line in Fig. 6(a), is higher than that of the HX1 (black solid line) at photon energies lower than 13.8 keV. When the photon energies at the HX1 and the HX2 are the same, the saturation power of the HX2 is similar to or a little lower than that of the HX1, as shown by the red dotted line in Fig. 6(a). As the two conditions represent the boundaries of the highest and the lowest performances at the HX2, we expect that a radiation power between those two values can be obtained from the HX2 according to the resonant photon energy at the HX1.

IV. TIME-DEPENDENT SIMULATION

The saturation lengths of the HX2 for two conditions are similar to each other, as shown by the red solid line and the red dotted line in Fig. 6(b). Although the saturation length of the HX2 is always longer than that of the HX1 (black solid line), the saturation length of the HX2 is still competitive for gaining sufficient radiation power in the post-saturation region. For example, the saturation lengths of HX1, HX2 and HX2 with the same photon energy as that of HX1 are about 50 m, 61 m and 65 m, respectively, at a 10-keV photon energy. This means that the required numbers of undulator segments are 10, 12 and 13, respectively. These values are reasonable for obtaining sufficient power gain in the post-saturation region, because the total number of undulator segments used in the PAL-XFEL is 20. At photon energies higher than 18 keV, however, the saturation length is longer

than the length of the undulator line (20 undulator segments; 100 m), and the radiation power cannot reach the saturation level at the HX2. However, this does not matter because it is far from the target photon energy of the HX2 (2∼10 keV). Note that the drift spaces between undulator segments are not included in the saturation length estimated by Ming Xie's fitting formula, so the saturation length has to be divided by the length of the undulator segment to estimate the required number of undulator segments for saturation.

The saturation power and the saturation length calculated by using Ming Xie's fitting formula are useful to estimate roughly the performance of the undulator line and are compatible with the simulation results at the saturation point. However, the length of undulator line is fixed at 120 m (20 undulator segments) in our case. Sometimes, the saturation occurs early in the undulator line, and the post-saturation region has to be considered. In some cases, saturation does not appear due to the long saturation length. Therefore, a time-dependent simulation [15] with an optimized tapering configuration [16–18] has to be carried out to evaluate the performance of the HX2 exactly. The methods and the results will be discussed in the next section.

The undulator lattice units of the HX1 and the HX2 used in the simulation [15] are described in Fig. 7. In both cases, the length of the undulator segment is about 5 m, and the length of the undulator lattice unit is about 6 m including the drift spaces. The drift spaces at both ends of the undulator are necessary for installing the devices to diagnose the status of the electron beam, to focus the transverse beam size of the electron beam, and to match the phase of the electron beam to the phase of the radiation. The amplitude of the quadrupole magnetic field is fixed at 3.12 T over the entire range of photon energies for strong focusing of the electron beam. The total numbers of undulator lattice units used in HX1 and HX2 are 20 each, so the total length of both undulator lines is about 120 m, including drift spaces.

At the PAL-XFEL, a combination of linear tapering and quadratic tapering is applied to compensate for the electron beam energy loss due to the wakefield and the FEL lasing [16–18]. The electron beam energy at the i-th undulator segment (E_{i}) can be described as follows:

$$E_i = \begin{cases} E_{\mathrm{init}} + \frac{\Delta E_{\mathrm{linear}}}{N_{\mathrm{tot}}} \cdot i & (i \le n_{\mathrm{quad,start}}), \\ E_{\mathrm{init}} + \frac{\Delta E_{\mathrm{linear}}}{N_{\mathrm{tot}}} \cdot i + \frac{\Delta E_{\mathrm{quadratic}}}{(N_{\mathrm{tot}} - n_{\mathrm{quad,start}})^2} \cdot (i - n_{\mathrm{quad,start}})^2 & (i \ge n_{\mathrm{quad,start}}). \end{cases} \tag{3}$$

E_{init} is the initial electron beam energy at the 1st undulator segment, $\Delta E_{\mathrm{linear}}$ is the total energy loss due to the wakefield effect, $\Delta E_{\mathrm{quadratic}}$ is the total energy loss due to FEL lasing, $n_{\mathrm{quad,start}}$ is the starting number of undulator segments with quadratic tapering and N_{tot} is the total number of undulator segments. Electron beam energy along the undulator line can be calculated and can be converted to the undulator parameter by using the resonance condition as follows:

$$K = \sqrt{2 \cdot \left(\frac{2\gamma^2 \lambda_{\mathrm{r}}}{\lambda_{\mathrm{u}}} - 1 \right)}. \tag{4}$$

The optimized undulator tapering configuration can be determined by scanning the parameters used in Eq. (3). Because N_{tot} is 20 for the HX1 and the HX2 and $\Delta E_{\mathrm{linear}}$ is fixed at −10 MeV, as determined by evaluating the wakefield effect, two parameters ($n_{\mathrm{quad,start}}, \Delta E_{\mathrm{quadratic}}$) are actually scanned for optimization.

For example, the results of tapering optimization for the 10-keV FEL at the HX2 is shown in Fig. 8. The final radiation power at the end of the undulator line according to $n_{\mathrm{quad,start}}$ and $\Delta E_{\mathrm{quadratic}}$ is shown in Fig. 8(a). The value of $n_{\mathrm{quad,start}}$ is displayed in the legend of the figure. The undulator tapering configuration that generates the highest radiation power at the end of undulator line is decided as the optimal configuration. The optimal undulator tapering configuration for each $n_{\mathrm{quad,start}}$ selected from Fig. 8(a) is shown in Fig. 8(b). In the case of the 10-keV FEL at the HX2, the optimal undulator tapering configuration can be determined when $n_{\mathrm{quad,start}}$ is 11 and $\Delta E_{\mathrm{quadratic}}$ is −60 MeV.

The optimal undulator tapering configuration is decided over the photon-energy range from 2 keV to 20 keV for the HX1 and the HX2 with two conditions by scanning the parameters related to the undulator tapering, and the results are shown in Fig. 9. As shown in Fig. 9(a), the radiation power at the end of the undulator line is higher than the saturation power, which is shown in Fig. 6(a), over most of the photon-energy range by virtue of the additional power gain in the post-saturation region. However, the radiation power at the HX2 is lower than the saturation power at photon energies higher than 17 keV because the saturation length is longer than the length of the undulator line, as shown in Fig. 6(b). Thus, the radiation power cannot reach the saturation level. $n_{\mathrm{quad,start}}$ for each optimized undulator tapering configuration is shown in Fig. 9(b). The higher the generated photon energy from the undulator line is, the longer the saturation length must be, and the later quadratic tapering is to be applied for all cases. The values of $n_{\mathrm{quad,start}}$ for the HX2 for the two conditions are always higher than that of the HX1 over the entire

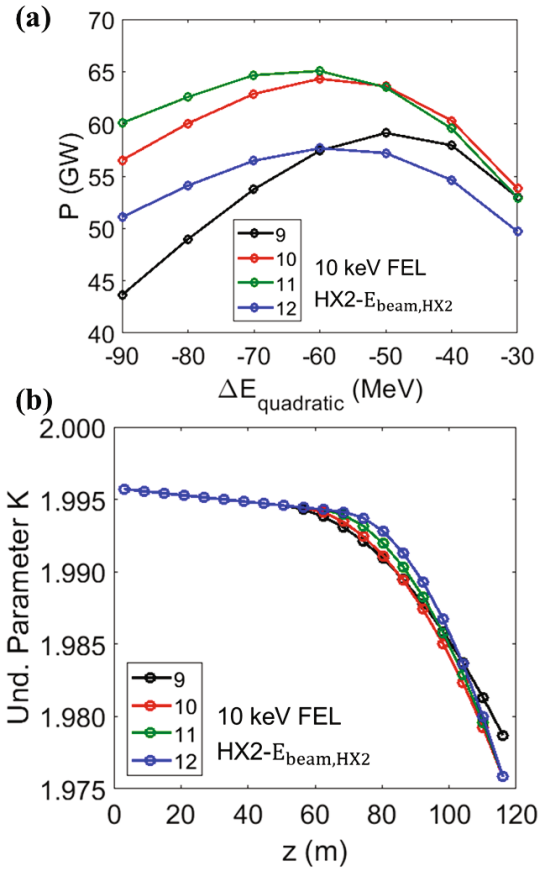

Fig. 8. Simulation results of tapering optimization for the 10-keV FEL at the HX2. (a) Radiation power at the end of undulator line vs. electron beam energy loss for quadratic tapering ($\Delta E_{\mathrm{quadratic}}$) for various starting points of quadratic tapering ($n_{\mathrm{quad,start}}$). (b) Optimal tapering configuration along the undulator line of the HX2 for each $n_{\mathrm{quad,start}}$ selected by using Fig. 8(a).

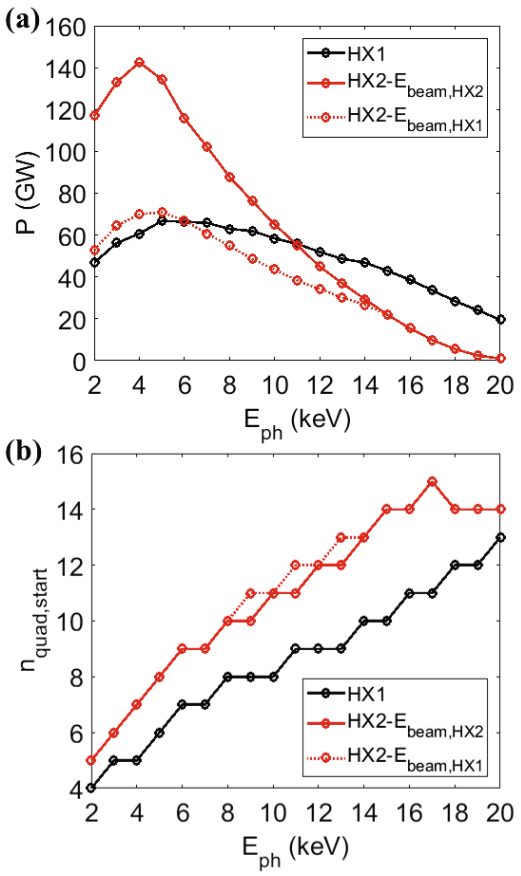

Fig. 9. (a) Radiation power at the end of undulator line with an optimized tapering configuration and (b) starting point of quadratic tapering ($n_{\mathrm{quad,start}}$) for an optimized tapering configuration vs. resonant photon energy for the HX1 (λ_{u} = 26 mm, black solid line) and for the HX2 (λ_{u} = 35 mm, red solid line). The red-dashed line indicates the HX2 with an electron beam energy for the same photon energy at the HX1. The optimal tapering configuration for each case is determined by using related-parameter scanning, which is introduced in Fig. 8.

range of photon energies because the saturation lengths for the HX2 for the two conditions are also longer than that of the HX1, as expected from Fig. 6(b).

The radiation power gain along the undulator line for representative photon-energy cases (2, 6, 10, 14 keV) in Fig. 9 are shown in Fig. 10. When the photon energy is 2.0 keV, the final radiation power of the HX2 (red solid line, Fig. 10(a)) is about 2.5 times higher than that of the HX1 (black solid line, Fig. 10(a)). Even though the growth of the radiation power of the HX2 starts later than it does for the case of the HX1, sufficient power gain in the post-saturation region is acquired by using a high electron beam energy. When the same photon energies are used simultaneously at the HX1 and the HX2, the growth of the radiation power also starts later than it does for the HX1, as shown by the red dotted line in Fig. 10(a). However, the final radiation power is a little higher than that of the HX1 as a sufficient length of the post-saturation region is reserved.

When the photon energy at 6.0 keV is generated at the HX2, the final radiation power (red solid line, Fig. 10(b)) is about 1.74 times higher than that of the HX1 (black solid line, Fig. 10(b)). The growth of the radiation power at the HX2 still starts later than it does at the HX1, and the radiation power of the HX2 overtakes that of the HX1 in the post-saturation region. When the same electron beam energies are used simultaneously at the two undulator lines with the same photon energies, the radiation power at the HX2 is increased to a level similar to that at the HX1 in spite of the late growth of the radiation power, as shown by the red dotted line in Fig. 10(b).

When the resonant photon energy is 10 keV, which is the highest photon energy of the target photon energy range at the HX2, the radiation power at the end of the undulator line of the HX2 (red solid line, Fig. 10(c)) is 1.11 times higher than that of the HX1 (black solid line, Fig. 10(c)). Although the electron beam energy

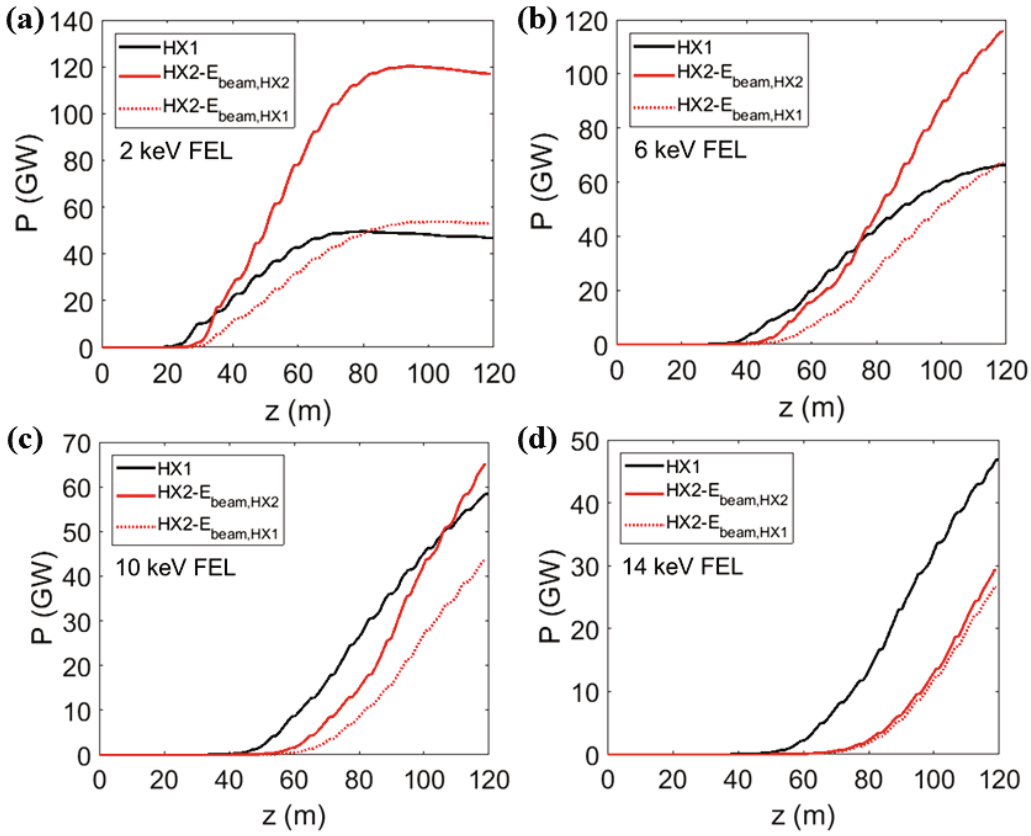

Fig. 10. Radiation power vs. z along the undulator line of (a) 2 keV, (b) 6 keV, (c) 10 keV, and (d) 14 keV for the HX1 (λ_u = 26 mm, black solid line) and for the HX2 (λ_u = 35 mm, red solid line). The red-dotted line indicates the HX2 with an electron beam energy for the same photon energy at the HX1.

for the HX2 is still higher by about 1.8 GeV than that for the HX1 as shown in Fig. 5(a), the final radiation power of the HX2 is slightly increased from that of the HX1 due to the shortfall of the undualtor length for the post-saturation region. When the two undulator lines are operated simultaneously with the same photon energy, the final radiation power at the HX2 (red dotted line, Fig. 10(c)) is about 0.75 times lower than that at the HX1 because of the low electron beam energy and the long saturation length.

When the resonant photon energy is 14 keV, the final radiation power of the HX2 is 0.63 times lower than that of HX1, as shown by the red and the black solid lines in Fig. 10(d). The growth of the radiation power at the HX2 still starts later than it does at the HX1, and the length of post-saturation region is too short to obtain sufficient power gain. Furthermore, a higher gain in the radiation power at the HX2 cannot be expected because the difference in the electron beam energies between the HX1 and the HX2 is only 0.24 GeV (HX1: 10.26 GeV; HX2: 10.5 GeV). When the same photon energies are generated simultaneously at the two undulator lines, the final radiation power at the HX2 is 0.57 times lower than that at the HX1.

From the estimate using Ming Xie's fitting formula [13,14], the graphs of the saturation powers at the HX1 and the HX2 cross at 13.8 keV, as shown in Fig. 6, when the post-saturation region is not considered. From the simulation [15] results with the optimized undulator tapering configuration [16–18], however, the cross point is moved to lower photon energy, about 11 keV, as shown in Fig. 9(a). By investigating the representative cases in Fig. 10, we figured out that a high electron beam energy is important for power enhancement. A sufficient undulator length for the post-saturation region is also important for obtaining additional power gain.

Therefore, the performance of the HX2 with a 35-mm undulator period for simultaneous operation can be described by dividing it into three ranges: (1) When a photon energy from 2 keV to 6 keV is provided from the HX2, the final radiation power of the HX2 is always higher than that of the HX1, regardless of the electron beam energy. (2) When a photon energy from 6 keV to 11 keV is used at the HX2, the final radiation power may or may not be higher than that of the HX1, depending on the photon energy of the HX1 (electron beam energy). (3) When a photon energy higher than 11 keV is generated from the HX2, the final radiation power of the HX2 is always lower than that of the HX1, regardless of the electron beam energy.

V. CONCLUSION

A new hard X-ray undulator line (HX2) at the PAL-XFEL is proposed, and the undulator period is decided as 35 mm by using Ming Xie's fitting formula [13,14] to estimate the performance of the HX2. Two boundary conditions for the HX2 are considered to fully identify its performance in regard to the simultaneous operation with the HX1: (1) The electron beam energy is increased as much as possible for the HX2. (2) The resonant photon energies at the HX1 and the HX2 are the same. FEL simulations [15] are also carried out to evaluate the performance of the HX2, including the effect of the post-saturation region. The undulator tapering configuration [16–18] is optimized by maximizing the FEL intensity for each case.

By utilizing an undulator with a longer period and a higher undulator parameter K, one can access a high electron beam energy at the HX2. Therefore, the radiation power at the end of the HX2 can be increased up to 2.5 times that of the HX1 over the entire target photon energy range of the HX2 ($2 \sim 10$ keV).

The layout of the HX2 will be optimized to make possible advanced schemes, such as self-seeding [20], an attosecond XFEL [21,22] and improved-SASE, at the HX2. The performance of such schemes will also be investigated to identify the scientific opportunities that may emerge at the HX2 in the future.

ACKNOWLEDGMENTS

This research was supported by the Basic Science Research Program through the National Research Foundation of Korea (NRF) funded by the Ministry of Education (Grant No. NRF-2019R1I1A1A01041573).

REFERENCES

[1] P. Emma *et al.*, Nat. Photonics **4**, 641 (2010).
[2] T. Ishikawa *et al.*, Nat. Photonics **6**, 540 (2012).
[3] H-S. Kang *et al.*, Nat. Photonics **11**, 708 (2017).
[4] M. Altarelli, Nucl. Instrum. Methods Phys. Res. B **269**, 2845 (2011).
[5] C. J. Milne *et al.*, Appl. Sci. **7**, 720 (2017).
[6] I. S. Ko *et al.*, Appl. Sci. **7**, 479 (2017).
[7] H-S. Kang *et al.*, J. Synchrotron Radiat. **26**, 1127 (2019).
[8] K. H. Kim *et al.*, Science **358**, 1589 (2017).
[9] S. H. Park *et al.*, Sci. Rep. **9**, 16316 (2019).
[10] J-H. Park *et al.*, Int. J. Mol. Sci. **20**, 1943 (2019).
[11] A. S. M. Ismail *et al.*, Phys. Chem. Chem. Phys. **22**, 2685 (2020).
[12] Z. Huang and K-J. Kim, Phys. Rev. ST Accel. Beams **10**, 034801 (2007).
[13] M. Xie, in *Proceedings of the 1995 Particle Accelerator Conference* (Dallas, USA, 1995), p. 183.
[14] M. Xie, Nucl. Instrum. Methods Phys. Res. A **445**, 59 (2000).
[15] S. Reiche, Nucl. Instrum. Methods Phys. Res. A **429**, 243 (1999).
[16] N. M. Kroll, P. L. Morton and M. N. Rosenbluth, IEEE J. Quantum Electron. **17**, 1436 (1981).
[17] Y. Jiao *et al.*, Phys. Rev. ST Accel. Beams **15**, 050704 (2012).
[18] A. Mak, F. Curbis and S. Werin, Phys. Rev. ST Accel. Beams **18**, 040702 (2015).
[19] D-E. Kim *et al.*, J. Korean Phys. Soc. **71**, 744 (2017).
[20] C-K. Min *et al.*, J. Synchrotron Radiat. **26**, 1101 (2019).
[21] Y. W. Parc, C. H. Shim and D. E. Kim, Appl. Sci. **8**, 1588 (2018).
[22] H-S. Kang and I. S. Ko, Nat. Photonics **14**, 7 (2020).